Desalination and Water Treatment
www.deswater.com
doi: 10.1080/19443994.2013.797546

52 (2014) 2502–2511
March

Taylor & Francis
Taylor & Francis Group

Design of a parabolic solar collector system for seawater desalination in Gaza

Juma Yousuf Alaydi

Mechanical Engineering Department, Islamic University, Gaza, Palestine
Email: jalaydi@iugaza.edu

Received 7 April 2012; Accepted 8 April 2013

ABSTRACT

This paper presents the design of a parabolic-trough solar collector system for seawater desalination in Gaza, collector-aperture and rim-angle optimization together with the receiver-diameter selection are presented. A comparison of concentrating collectors against conventional flat-plate collectors is presented. It is shown that for large-scale water production the parabolic-trough collectors are more efficient than the flat plate ones. The analysis considers visible radiation transfer, IR radiation exchange, conductive and convective losses, and energy transfer to a fluid flowing through the collector tube. The collector may have a tilted north-south axis, an east-west axis or it may fully track the sun and geometric parameters associated with tracking the sun are considered.

Keywords: Solar desalination; Parabolic-trough collectors; Solar radiation

1. Introduction

Gaza enjoys an abundance of solar radiation. The mean daily global solar radiation varies from about 2–3 kWh/m^2 in the cloudiest months of the year (i.e. December and January) to about 8 kWh/m^2 in July. [1,2]. The annual global solar-radiation received on a horizontal surface, for average weather conditions, is 1,725 kWh/m^2, 69% of this amount, (i.e. 1,188 kWh/m^2) reaches the surface as direct solar radiation and the rest, 31% (i.e. 537 kWh/m^2), as diffuse radiation. According to Marinos et al. [3] and Morris and Hanbury [4], the worldwide installed capacity of desalinated water systems in 1990 reached 13 million m^3/day, which, by the year 2010, is expected to double. The dramatic increase in desalinated water supply will create a series of problems, the most significant of which are those related to energy consumption. It has been estimated that a production of 13 million m^3 of portable water per day requires 130 million tons of oil per year. If desalination is accomplished by conventional technology, then it will require the burning of substantial quantities of fossil fuels. Given that conventional sources of energy are polluting, sources of energy that are not polluting will have to be used. Fortunately, there are many parts of the world that are short of water but have exploitable renewable-energy sources that could be used to drive desalination processes.

Solar desalination is used in nature to produce rain, which is the source of freshwater supply. Solar radiation falling on the surface of the sea is absorbed as heat and causes evaporation of the water. The vapor rises above the surface and is moved by winds. When this vapor cools down to its dew point, condensation occurs and freshwater precipitates as rain.

Solar energy can be used for seawater desalination either by producing the thermal energy required to drive the phase-change processes or by generating the electricity required to drive the membrane processes. Solar-desalination systems are thus classified into two categories, i.e. direct and indirect collection systems. As their name implies, direct collection systems use solar energy to produce distillate directly in the solar collector, whereas in indirect collection systems, two sub-systems are employed (one for solar energy collection and one for desalination). Conventional desalination (http://www.sciencedirect.com/science/article/pii/S030626199800018X#hit54) systems are similar to solar systems because the same type of equipment is applied. The prime difference is that in the former, either a conventional boiler is used to provide the required heat or main electricity is used to provide the required electric power, whereas in the latter, solar energy is applied.

The solar parabolic trough collector (PTC) model is presented in this paper. The tracking mechanism consists of a low-speed 12V d.c motor and a control system. The input signals to the control system are obtained from three light-dependent resistors. One resistor determines whether the collector is in focus, the second determines the sun/cloud condition, while the third whether it is day or night, where the accuracy of the mechanism is also presented.

2. Solar collector design

From the many types of solar collectors developed, three types of merit further consideration for steam generation: the PTC, the compound parabolic collector (CPC), and the flat-plate collector (FPC). The first one is a tracking collector, whereas the last two are stationary. PTCs are generally of medium concentration ratio (15–40) whereas CPCs are generally of low concentration ratios (1.5–5). The low concentration ratios of the latter allow them to work without a need for tracking of the Sun.

2.1. Collector type selection

In general, concentrating collectors exhibit certain advantages as compared with the conventional flat-plate type. The main ones are:

(1) The working fluid can achieve high temperatures in a concentrator system when compared with a flat-plate system of the same (http://www.sciencedirect.com/science/article/pii/S030626199800018X#hit116) solar-energy collecting surface. This means that a higher thermodynamic efficiency can be achieved.
(2) It is possible with a concentrator system to achieve a thermodynamic match between temperature level and task. The task may be to operate thermionic, thermodynamic, or other higher temperature devices.
(3) The thermal efficiency is greater because of the small heat-loss area relative to the receiver area.
(4) Reflecting surfaces require less material and are structurally simpler than flat-plate collectors. For a concentrating collector, the cost per unit area of the solar collecting surface is therefore less than that of a flat-plate collector.
(5) Owing to the relatively small area of receiver per unit of collected solar energy, selective surface treatment and vacuum insulation to reduce heat losses and improve the collector efficiency are often economically viable.

Their disadvantages are:

(1) Concentrator systems collect little diffuse radiation, the rate depending on the concentration ratio.
(2) Some form of tracking system is required, so as to enable the collector to follow the Sun.
(3) Solar-reflecting surfaces may lose their reflectance with time and may require periodic cleaning and refurbishing.

Perhaps their most important advantage is the enhanced thermal-efficiency and therefore this is further analyzed. The thermal efficiency of a concentrating collector is defined as the ratio of the useful energy delivered to the energy incident at the concentrator aperture. This may be calculated from an energy balance on the receiver [5,6] which is given by:

$$n = n_o - \left(\frac{U_L(T_r - T_a)}{1 * CR}\right) \quad (1)$$

or in terms of the heat-removal factor:

$$n = F_R\left(n_o - \frac{U_L(T_i - T_a)}{1 * CR}\right) \quad (2)$$

From both equations, it can be concluded that the efficiency of a concentrating collector depends on the optical efficiency (n_o) which is determined by the optical properties of various materials used in the construction of the collector and the magnitude of the

heat losses, as indicated by the second term in Eq. (1). The advantage of concentrating collectors is that the heat losses are inversely proportional to the concentration ratio (CR). The standard collector-performance can be indicated by the corresponding straight line, whose slope and intercept are the indications of performance as shown in Eq. (3):

$$n = I_n - S\left(\frac{\Delta T}{I}\right) \quad (3)$$

where $I_n = \text{intercept} = F_R\ n_o$ and $S = \text{slope} = F_R U_L / CR$ and I is solar beam radiation (W/m^2).

The same relations apply to a flat-plate collector, in which case $CR = 1$. The small heat-loss term in Eqs. (1) and (2) for the parabolic trough collector leads to a small slope of the typical collector–performance curve, Fig. 1 this does not apply for flat-plate collectors. This means that the efficiency in the PTCs remains high at high inlet water temperatures. Therefore, at a temperature of 100 ℃, which occurs at a $\Delta T/I$ value of about 0.1, PTCs work at an efficiency of about 62%, CPCs at about 32% and the FPC at about 10%. This clearly suggests that the PTC is the best type of collector for this application.

2.2. Parabolic trough collector design

Parabolic trough collectors are employed in a variety of applications, including industrial steam production [7] and hot water production [8].

Fig. 2 shows schematic of a parabolic trough collector. These are preferred for solar steam generation because, as was seen above, high temperatures can be obtained without any serious degradation of the collector efficiency. In this paper, PTCs are used for purified water production by producing the steam used to power a MEB evaporator.

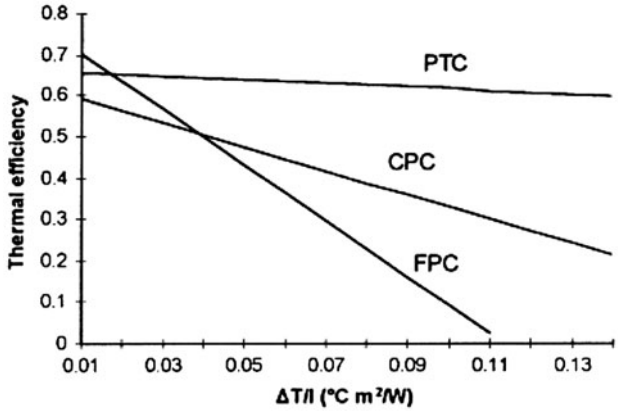

Fig. 1. Typical collector–performance curves.

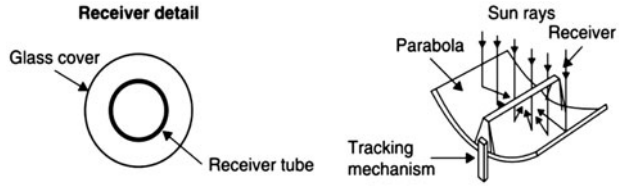

Fig. 2. Schematic of a parabolic trough collect.

Table 1
Parabolic trough collector specifications

Item	Value or type
Collector's aperture-area	10–2, 160 m^2
Collector's aperture	1.46 m
Aperture-to-length ratio	0.64
Rim angle	90
Glass-to-receiver ratio	2.17
Receiver diameter	22 mm
Concentration ratio	21.2
Collector's test intercept	0.638
Collector's test slope	0.387 W/m^2K
Tracking mechanism collector type	Electronic
Mode of tracking	E–W horizontal
Mass flow rate	0.012 $kg/s\,m^2$

The design of the parabolic trough collector system is detailed in Kalogirou et al. [9] and Kalogirou [10]. Four sizes of applications are analyzed here, with aperture area, varying from 10–2,160 m^2. The specifications of the collector are shown in Table 1. The same collector characteristics are applicable to all the collector sizes employed.

3. Design of the steam generation method

Three methods have been employed to generate steam using parabolic-trough collectors:

(1) The direct or in situ concept in which two-phase flow is allowed in the collector receiver, so that steam is generated directly.
(2) The steam-flash concept, in which pressurized water is heated in the collector and then flashed to steam in a separate vessel.
(3) The unfired-boiler concept, in which a heat-transfer fluid is circulated through the collector and hence steam is generated via heat-exchange in an unfired boiler.

These steam-generation methods were analyzed with respect to the system's simplicity, capital cost and stability [11].

It can be said that water-based systems are simpler and safer for desalination. With proper selection of flow rate and the desalination-system's steam-supply pressure, the pump power can be kept to a minimum. This reduces the main disadvantage of the steam-flash system against the in situ system: as their costs are similar, the steam-flash system is selected. For a maximum value of solar radiation of 1,000 W/m^2, the outlet temperature of the water, for a 100 ℃ inlet temperature (i.e. the pressure in the separator being equal to atmospheric and the flow rate equal to 0.012 kg/s m^2) would be 120 ℃. This is considered a reasonable value, not causing the collector to work at excessively high temperatures, and only requires a pressure of 2 bar to avoid boiling.

3.1. Flash-vessel design

In order to separate steam at a lower pressure, a flash vessel is used. This is a vertical vessel as shown in Fig. 3, with the inlet for the water located about one third of the way up its side. The standard design of flash vessels requires that the diameter of the vessel is chosen so that the steam flows towards the top outlet connection at no more than about 3 m/s. This should ensure that any water droplets can fall through the steam (i.e. in contra-flow), to the bottom of the vessel. Adequate height above the inlet is necessary to ensure separation. The separation is also facilitated by having the inlet projecting downwards into the vessel. The water-outlet connection is sized to minimize the pressure drop from the vessel to the pump inlet to avoid cavitation. The flash valve connected to the vessel inlet is spring loaded for adjustment purposes.

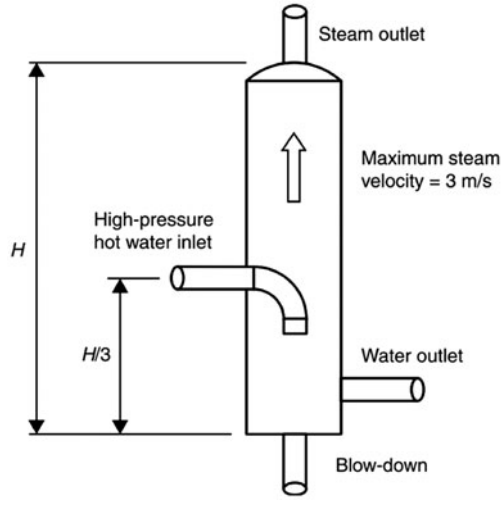

Fig. 3. Flash vessel schematic diagram.

In order to maximize the system's steam production, the heat-up energy requirements should be kept to a minimum. This is because energy invested in the preheating of the flash vessel is inevitably lost due to the nature of the diurnal cycle. The losses during overnight or shut-down return the vessel to near ambient conditions every morning. This could be readily achieved by optimizing the flash-vessel's water inventory and dimensions in order to lower the system's thermal capacity and losses. The following constraints on the optimization should be noted, however:

(1) The mass of the circulating water contained in the pipes cannot be changed.
(2) The water inventory in the flash vessel should not be reduced below a certain level, because the system's performance will deteriorate. The addition of make-up water, which is continuously supplied to keep the water level in the flash vessel constant, would then "dilute" the system temperature and possibly result in instabilities [12].

The height of the flash vessel should also be kept to a minimum, which in combination with the right steam velocity would avoid the possibility of "contamination" of the steam with water droplets (i.e. carry-over). Furthermore, a reduced vessel height and hence a consequent reduction in the system's thermal capacity, will lead to a faster response of the system. In an earlier report [13], the problem of system optimization through variation of the flash-vessel's design was studied in detail. The optimal flash vessel design parameters for a system with a collector area of 10 m^2 are shown in Fig. 3.

4. Design of the desalination system

4.1. System circuit arrangement

The circuit must be able to carry the seawater from the sea to the MEB evaporator and return the rejected brine back to the sea. These two streams must be remote from each other to avoid potential mixing problems. The circuit diagram, shown in Fig. 4, gives details of only the intake stream. Whenever possible, the intake from a well next to the coast line is preferred because as the water passes through the sand it is filtered. The water, after passing through a filter is directed to the MEB evaporator's last effect, to cool the steam produced in the previous effect. Part of this water is then returned to the sea as warm brine and part as feed water directed to the evaporator's top effect after a scale inhibitor is ejected. In Fig. 4, the solar collectors and the

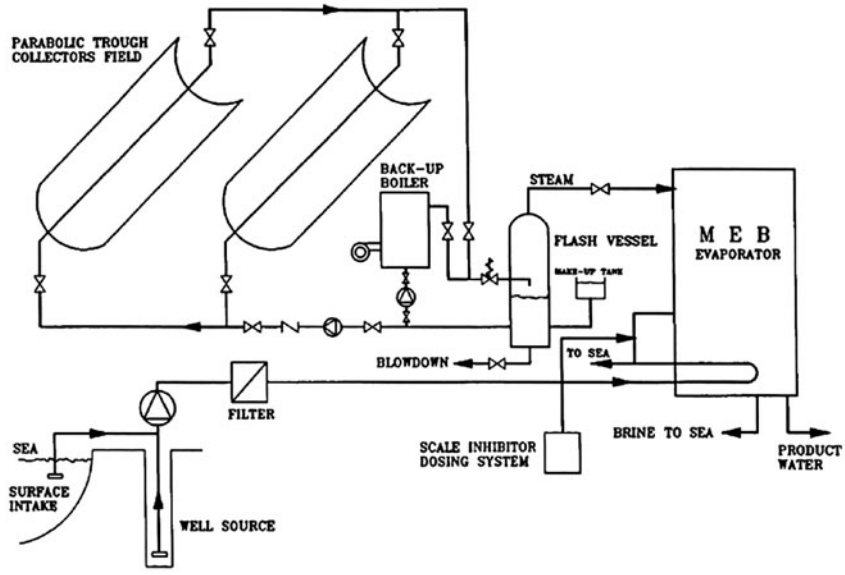

Fig. 4. System circuit arrangement.

steam-generation system-piping layout is also shown. A back-up boiler is also shown in Fig. 4. This is necessary for the operation of the evaporator during days of low insulation and/or during the night. As can be seen from Fig. 4 no complicated controllers are required. This is because the steam delivery temperature is constant (i.e. dependent on the evaporator pressure) and the operation of the boiler can be controlled by a simple thermostat located at the pipe before the flash vessel. The same principle applies for the operation of the boiler during day-time (back-up of the solar system) and night-time.

4.2. Evaporator design

Of the various types of MEB evaporators, the Multiple Effect Stack (MES) type is the most appropriate for solar energy application. This features several advantages, the most important of which is the stable operation between virtually zero and 100% output, even when sudden changes are made, as well as its ability to follow a varying steam supply without upset. In Fig. 5, a four-effect MES evaporator is shown. Seawater is sprayed into the top of the evaporator and descends as a thin film over the horizontally arranged tube-bundle in each effect.

In the top (hottest) effect, steam from the solar collector system condenses inside the tubes. Because of the low pressure created in the plant by the vent ejector system, the thin seawater film boils on the outside of the tubes, so creating new vapor at a lower temperature than the condensing steam.

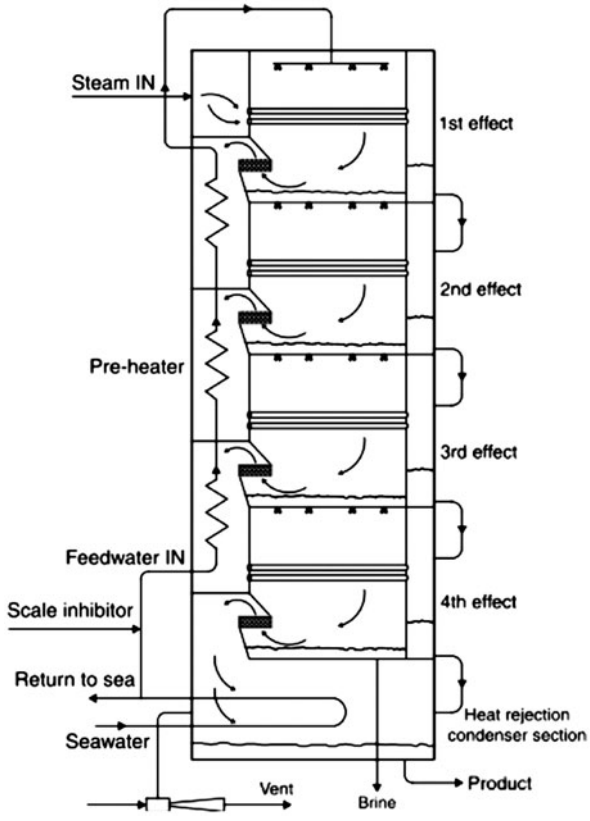

Fig. 5. Four-effect MES evaporator.

The seawater falling to the floor of the first effect is cooled by flashing through nozzles into the second effect, which is at a lower pressure. The vapor made in the first effect is ducted into the inside of the tubes

in the second effect, where it condenses to form part of the product. Again, the condensing warm vapor causes the cooler external seawater film to boil at the reduced pressure.

The evaporation–condensation process is repeated from effect-to-effect down the plant, creating an almost equal amount of product inside the tubes of each effect. The vapor made in the last effect is condensed on the outside of a tube bundle cooled by raw seawater. Most of the warmer seawater is then returned to the sea, and a small part is used as feed water to the plant. After being treated with acid to destroy scale-forming compounds, the feed water passes up the stack through a series of pre-heaters that use a little of the vapor from each effect to gradually raise its temperature, before it is sprayed into the top of the plant. The water produced from each effect is flashed in cascade down the plant so that it can be withdrawn in a cool condition at the bottom of the stack. The concentrated brine is also withdrawn at the bottom of the stack.

The MES process is completely stable in operation and automatically adjusts to changing steam conditions, even if they are suddenly applied, so it is suitable for load following applications. It is a once-through process that minimizes the risk of scale formation without incurring a large chemical scale dosing cost. The typical product purity is less than 5 ppm TDS and does not deteriorate as the plant ages. Therefore, the MEB process and in particular the MES-type evaporator appears to be the most suitable to be used with solar energy.

5. System modeling

The modeling program is used to predict the quantity of the steam produced by the collector and the flash vessel, and subsequently the amount of desalinated water produced by the various systems. The principle of operation of the program is that it employs the values of the solar radiation and ambient-air temperature from a reference year developed previously. The values of the solar radiation are corrected hourly for the collector's inclination.

In the analysis, a representative day for each month is taken as shown in Table 2 http://www.sciencedirect.com/science/article/pii/S0306261998000-18X-tbl5. These are chosen because the value of extraterrestrial solar radiation is closest to the month's average for that day [14].

In the program, the actual measured collector performance parameters of test slope and intercept are required. These were obtained by testing the collector according to the procedures outlined in ASHRAE Standard 93 [15].

Table 2
Average day of each month

Month	Day	Month	Day
January	17	July	17
February	16	August	16
March	16	September	15
April	15	October	15
May	15	November	14
June	11	December	10

The program takes into account, in addition to the sensible heat and the thermal capacity of all the system components, all the heat losses from the system i.e. the flash-vessel body, pipes, and pump body. After all these losses are estimated, the flash-vessel's inlet water temperature is determined. From the difference in enthalpy of this hot water from that of the water contained in the flash vessel, i.e. the steam production is calculated. The accuracy of the simulation depends to a great extent on the validity of the reference year. This was investigated when modeling the performance for hot water production from PTCs [16].

Although the variation reported was 7%, this cannot be generalized as an expected variation. Details about the structure of the program and the validation of the model are given in Kalogirou et al. [17]. The rate of freshwater produced by the desalination system is evaluated by using the evaporator performance ratio figure. Several systems were considered in this study with aperture areas varying from small 10 m^2 to large 2,160 m^2. The smallest system is suitable for supplying water in a block of 3–4 houses and the largest for a village of about 400 persons. The modeled performances of the systems are shown in Table 3.

By studying Table 3, it can be seen that the system's performance is in phase with the weather, i.e. during periods of dry weather (summer) the system's production is at its greatest. This is considered to be the most important advantage of solar desalination.

6. Optimization of the rim angle

The rim angle ($\emptyset_r$) is the angle from the rim of the collector to the line normal to the collector surface passing through the focus. Fig. 6 shows that, for the same aperture, various rim angles are possible. It also shows that, for different rim angles, the focus-to-aperture ratio which defines the curvature of the parabola is changing. It can be demonstrated that,

Table 3
The modeled performances of the systems

Month	System production (litres/month)			
	Area = 8 m^2	Area = 50 m^2	Area = 450 m^2	Area = 2,000 m^2
January	24	118	1,914	8,613
February	43	262	3,594	15,392
March	135	952	8,878	45,639
April	192	1,375	15,772	63,803
May	252	1,796	20,392	82,465
June	370	2,703	30,087	121,285
July	398	2,919	32,415	130,748
August	351	2,592	28,841	116,281
September	273	2,027	22,690	91,578
October	149	1,099	12,656	51,362
November	64	435	5,458	22,491
December	30	179	2,597	11,955

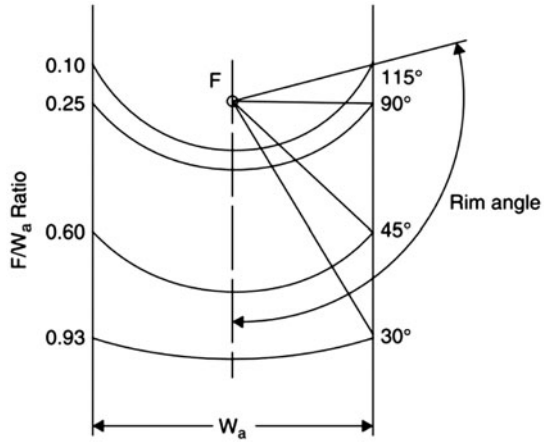

Fig. 6. Rim angle.

with a 90° rim angle, the mean focus to reflector distance and hence the reflected beam spread is minimized, so that the slope and tracking errors are less pronounced. [5] The collector's surface area decreases as the rim angle is decreased. There is a temptation to use smaller rim angles because there is only a small sacrifice in optical the cost of the reduction in the performance with the small decrease in optical efficiency is greater than the saving in material area. The rim angle was finally selected to be 90°.

7. Selection of the receiver diameter

The receiver diameter determines the intercept factor and consequently the optical efficiency. The intercept factor is the ratio of the energy intercepted by the receiver to the total energy reflected by the focusing device [18]. Its value depends on the size of the receiver, the surface angle errors of the parabolic mirror, and the solar beam spread. These errors are identified as apparent changes of the Sun's width, scattering effects associated with the reflective surface, and scattering effects caused by random slope errors (i.e. distortion of the parabola due to wind loading). Nonrandom errors account for the errors in the manufacture/assembly and/or in the operation of the collector. These are identified as reflected profile errors, misalignment errors and receiver location errors [6]. Random errors are modeled statistically, by total reflected-energy distribution standard deviations at normal incidence [6].

$$\sigma = \sqrt{\sigma_{\text{sun}}^2 + 4\sigma_{\text{slope}}^2 + \sigma_{\text{mirror}}^2} \tag{4}$$

Nonrandom errors are determined by the misalignment angle error β (i.e. the angle between the reflected ray from the center of the Sun and the normal to the reflector's aperture plane) and the receiver mislocation distance dr. As reflector profile errors and receiver mislocation along the Y-axis essentially have the same effect, this parameter is used to account for both. According to Guven and Bannerot, [6] random and nonrandom errors can be combined with the collector's geometric parameters, CR and receiver diameter (D), to yield error parameters universal to all collector geometries. These are called 'universal error parameters' and an asterisk is used to distinguish them from the already defined parameters. Using the universal error parameters, the formulation of the intercept factor γ is possible from Eq. (6) [7].

$$\gamma D = \frac{1+\cos\phi_r}{2\sin\phi_r}\int_0^{\phi_r} Erf\left(\frac{\sin\phi_r(1+\cos\phi)(1-2d^*\sin\phi)-\pi\beta^*(1+\cos\phi_r)}{\sqrt{2}\pi\sigma^*(1-\cos\phi_r)}\right) - Erf\left(-\frac{\sin\phi_r(1+\cos\phi)(1+2d^*\sin\phi)+\pi\beta^*(1+\cos\phi_r)}{\sqrt{2}\pi\sigma^*(1-\cos\phi_r)}\right)\frac{d\phi}{(1+cos\phi)} \quad (5)$$

For the evaluation of the intercept factor, a computer program was written. The principle of operation of the program is that the two error functions within the integral are estimated for each step of angle ϕ and then the integral is numerically evaluated using Simpson's integration method.

For a carefully fabricated collector, [6] $\sigma_{\text{mirror}} = 0.002$ rad and $\sigma_{\text{slope}} = 0.004$ rad. The standard distribution of the Sun's intensity distribution can be taken as 0.0025 rad. Therefore σ (in radians) is given by:

$$\sigma = \sqrt{(0.0025)^2 + 4(0.004)^2 + (0.002)^2} = 0.00861 \quad (6)$$

$\beta = 0.2^\circ = 0.0035$ rad (i.e. the maximum tracking error), [6].

Using these inputs, together with various receiver diameters, the results shown in Table 4 were obtained. Certainly the aim is towards a high intercept factor. From Table 4 the selection of the receiver diameter could be either 12 or 15 mm. The final selection would depend, however, on the thermal analysis. This is because the larger diameter gives a higher intercept factor but simultaneously higher thermal losses. The results of the thermal analysis are shown in Table 5, it can be seen that the thermal efficiency is maximum for the 12 mm-diameter receiver, which is naturally selected.

Table 4
Intercept factors for various receiver diameters

Receiver diameter (mm)	CR	Intercept factor
6	42.44	0.80
9	28.29	0.94
12	21.22	0.98
15	16.98	0.99
18	14.15	1.00
21	12.13	1.00

Table 5
Thermal efficiency as a function of receiver diameter

Receiver diameter (mm)	Optical efficiency	Thermal efficiency
6	0.529	0.496
9	0.618	0.568
12	0.648	0.582
15	0.661	0.579
18	0.661	0.562
21	0.661	0.545

8. Tracking

Fig. 7 shows the system, which was designed to operate with the required tracking accuracy, consists of a small direct current motor that rotates the collector via a speed reduction gearbox. A diagram of the system, together with a table showing the functions of the control system, is presented in Fig. 7. The system employs three sensors, of which A is installed on the east side of the collector shaded by the frame, whereas the other two (B and C) are installed on the collector frame. Sensor A acts as the "focus" sensor, i.e. it receives direct sunlight only when the collector is focused. As the sun moves, sensor A becomes shaded and the motor turns "on". Sensor B is the "cloud" sensor, and cloud cover is assumed when illumination falls below a certain level. Sensor C is the "daylight" sensor. The condition when all three sensors receive sunlight is translated by the control system as daytime with no cloud passing over the sun and the collector in a focused position. The functions shown in the

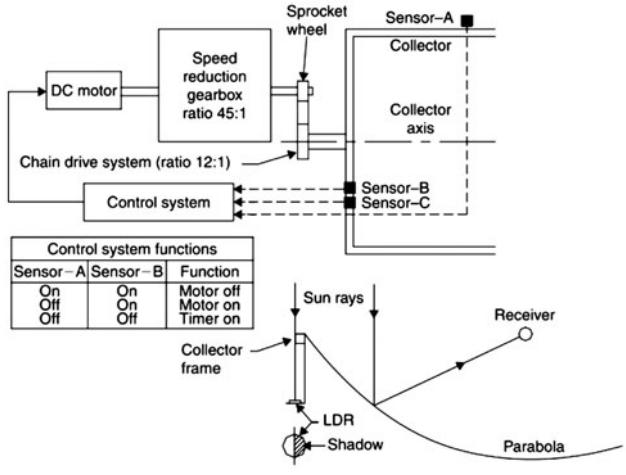

Fig. 7. PTC with tracking system.

table of Fig. 7 are followed provided that sensor C is "on", i.e. it is daytime. The sensors used are light-dependent resistors (LDRs).The main disadvantage of LDRs is that they cannot distinguish between direct and diffuse sunlight. However, this can be overcome by adding an adjustable resistor to the system, which can be set for direct sunlight (i.e. a threshold value). This is achieved by setting the adjustable resistor so that for direct sunlight, the appropriate input logic level (i.e. 0) is set.

As mentioned previously, the motor of the system is switched on when any of the three LDRs is shaded. The sensor which is activated depends on the amount of shading determined by the value set on the adjustable resistor, i.e. threshold value of radiation required to trigger the relays. Sensor A is always partially shaded. As the shading increases due to the movement of the sun, a value is reached that triggers the forward relay, which switches the motor on to turn the collector and therefore re-exposes sensor A. The system also accommodates cloud cover, i.e. when sensor B is not receiving direct sunlight, determined by the value of another adjustable resistor, a timer is automatically connected to the system and this powers the motor every 2 min for about 7s. As a result, the collector follows approximately the sun's path and when the sun reappears the collector is re-focused by the function of sensor A.

The system also incorporates two limit switches, the function of which is to stop the motor from going beyond the rotational limits. These are installed on two stops, which restrict the overall rotation of the collector in both directions, east and west. The collector tracks to the west as long as it is daytime. When the sun goes down and sensor C determines that it is night, power is connected to a reverse relay, which changes the motor's polarity and rotates the collector until its motion is restricted by the east limit switch. If there is no sun during the following morning, the timer is used to follow the sun's path as under normal cloudy conditions. The tracking system just described, comprising an electric motor and a gearbox, is for small collectors. For large collectors, powerful hydraulic units are required.

9. Conclusions

Solar desalination can be viable for two bigger installations considered. The unit water cost is insensitive to changes in the method of payment or to variations in direct costs. However, it is not usually worth operating the desalination system solely on solar energy due to the high cost of the desalination system and the high percentage of inactive time.

The author believes that even in cases where the fuel only systems result in lower or equal water prices compared with a solar plus fuel system, the solar alternative should not be abandoned because as it was proven a possible increase in fuel price turns the system viability in favor of the solar system. The issues of global warming and climate change resulting from the increase in greenhouse gases due to the burning of fuels should not be underestimated.

The design of a PTC system has been accomplished by performing an optimization of the collector's aperture and rim angle and the selection of the receiver's diameter. The last parameter was selected by examining the various errors encountered in the manufacture and/or operation of the system.

Nomenclature

PTC	—	parabolic trough collector
FPC	—	flat plate collector
CPC	—	compound parabolic collector
ER-RO	—	energy recovery-reverse osmosis
MEB	—	multiple effect boiling (evaporator)
MES	—	multiple effect stack (evaporator)
MSF	—	multiple effect flash (evaporator)
RO	—	reverse osmosis
ppm	—	parts per million
VC	—	vapor compression
PR	—	performance ratio
CR	—	concentration ratio
F_R	—	heat removal factor
I	—	beam solar radiation (W/m^2)
I_n	—	test intercept of collector performance graph
N	—	number of years
n_o	—	optical efficiency
n	—	thermal efficiency
S	—	test slope of the collector's performance graph
T_a	—	ambient temperature (K)
T_i	—	collector's inlet temperature (K)
T_r	—	mean receiver temperature (K)
U_L	—	steady-state heat loss coefficient (W/m^2K)
DT	—	temperature difference ($T_i - T_a$) (K)

References

[1] M.A.S. Malik, G.N. Tiwari, A. Kumar, M.S. Sodha, Solar Distillation, Pergamon Press, Oxford, 1985.
[2] A.B. Meinel, M.P. Meinel, Applied Solar Energy—An Introduction, Addison–Wesley, Boston, MA, 1976.

[3] D. Marinos, D. Assimacopoulos, F. Provatas, The experience of local authorities with water desalination in the Islands of Southern Europe, in: Proceedings of the New Technologies for the Use of Renewable Energy Sources in Water Desalination, Athens, Greece, Section V, 1991, pp. 48–56.
[4] R.M. Morris, W.T. Hanbury, Renewable energy and desalination—A review, in: Proceedings of the New Technologies for the Use of Renewable Energy Sources in Water Desalination, Athens, Greece, Section I, 1991, pp. 30–50.
[5] J.A. Duffie, W.A. Beckman, Solar engineering of thermal processes, 2nd ed, Wiley, New York, 1991.
[6] H.M. Guven, R.B. Bannerot, Determination of error tolerances for the optical design of parabolic troughs for developing countries, Solar Energy 36(6) (1986) 535–550.
[7] H.M. Guven, R.B. Bannerot, Derivation of universal error parameters for comprehensive optical analysis of parabolic troughs, Proceedings of the ASME-ASES Solar Energy Conference, Knoxville, TN, 1985, pp. 168–74.
[8] F. Kreith, J.F. Kreider, Principles of Solar Engineering, McGraw–Hill, New York, 1985.
[9] L.M. Murphy, K.E. May, Steam generation in line-focus solar collectors: A comparative assessment of thermal performance, operating stability, and cost, issues, SERI/TR-1311, 1982.
[10] S. Lloyd, Use of solar parabolic trough collectors for hot water production in Cyprus feasibility study, Renewable Energy Journal 2(2) (1992) 117–124.
[11] P. Eleftheriou, S. Lloyd, S. Kalogirou, J. Ward, Design and performance characteristics of a parabolic-trough solar-collector system, Appl. Energy 47 (1994) 341–354.
[12] S. Kalogirou, Parabolic-trough collector system for low temperature steam generation-design and performance characteristics, Appl. Energy 57(6) (1996) 1–19.
[13] P. Hurtado, M. Kast, Experimental Study of Direct in-situ Generation Line Focus Solar Collector, SERI, 1984.
[14] S. Kalogirou, P. Eleftheriou, S. Lloyd, J. Ward, Optimization of the initial response of a solar steam generation plant, in: Proceedings of the 1995 ASME/JSME/JSES International Solar Energy Conference, Maui, HI, 1995, pp. 513–520.
[15] A. Meaburn, F.M. Hughes, A simple predictive controller for use on large scale arrays of parabolic trough collectors, Solar Energy 56(6) (1996) 583–595.
[16] ASHRAE Standard, Methods of testing to determine the thermal performance of solar collectors. ANSI/ASHRAE, Ann Arbor, MI, 93, 1986.
[17] S. Kalogirou, S. Lloyd, J. Ward, Modeling of a parabolic trough collector system for hot-water production, Proceedings of the ISES Solar World Congress, Budapest, pp. 145–150 1993.
[18] E. Zarza, JL. Ajona, J. Leon, K. Genthner, A. Gregorzewski, Solar thermal desalination project at the Plataforma Solar De Almeria, in: Proceedings of the Biennial Congress of the International Solar Energy Society, Denver, CO., Vol. 1, Part II, 1991, pp. 2270–2275.